Circular Dichroism in Photoionization of H_2

D. Dowek,[1] J. F. Pérez-Torres,[2] Y. J. Picard,[1] P. Billaud,[1] C. Elkharrat,[1] J. C. Houver,[1] J. L. Sanz-Vicario,[3] and F. Martín[2]

[1]*Institut des Sciences Moléculaires d'Orsay (FRE 3363 Université Paris-Sud et CNRS), Bat 350, Université Paris-Sud, 91405 Orsay Cedex, France*

[2]*Departamento de Química, Módulo 13, Universidad Autónoma de Madrid, 28049 Madrid, Spain*

[3]*Grupo de Física Atómica y Molecular, Instituto de Física, Universidad de Antioquia, Medellín, Colombia*

(Received 23 March 2010; published 8 June 2010)

Circular dichroism is a consequence of chirality. However, nonchiral molecules can also exhibit it when the measurement itself introduces chirality, e.g., when measuring molecular-frame photoelectron angular distributions. The few such experiments performed on homonuclear diatomic molecules show that, as expected, circular dichroism vanishes when the molecular-frame photoelectron angular distributions are integrated over the polar electron emission angle. Here we show that this is not the case in resonant dissociative ionization of H_2 for photons of 30–35 eV, which is the consequence of the delayed ionization from molecular doubly excited states into ionic states of different inversion symmetry.

DOI: 10.1103/PhysRevLett.104.233003 PACS numbers: 33.20.Xx, 33.80.−b, 42.65.Re

The most recent advances in multicoincidence detection methods [1], in which the momentum of all charged particles is fully determined, are currently used to challenge the predictions of quantum theory to an unprecedented degree of accuracy. For example, recent observations supported by accurate theoretical calculations have shown that fixed-in-space homonuclear diatomic molecules behave as Young's double slits when the former are ionized by high-energy photons [2–5]. They have also shown that interferences can be responsible for symmetry breaking in symmetric molecules [6–8]. In most experiments, the use of linearly polarized light with a well-defined orientation with respect to the internuclear axis restricts the study of these interferences to states of a given molecular symmetry. However, more complex effects and, therefore, more challenging for experiment and theory, can be expected if one uses circularly polarized light that, in the case of diatomic molecules, leads to a coherent excitation of Σ and Π states.

One of these effects is circular dichroism, which measures the different responses of a molecule when exposed to left- or right-handed circularly polarized light. This phenomenon is usually associated with chiral molecules and is often used to characterize the structure of the corresponding enantiomers [9]. However, as anticipated in early theoretical studies [10–12], circular dichroism can also be observed in the photoionization of oriented achiral molecules. This is the result of the noncoplanarity of three vectors, namely, the light propagation axis of circularly polarized light $\mathbf{k}$, the photoelectron momentum $\mathbf{k}_e$, and the molecular axis $\mathbf{n}$ [see Fig. 1(a)]. The first experimental demonstration was reported by Westphal *et al.* [13,14], who studied valence and inner shell photoionization of CO molecules adsorbed on a surface with a well-defined orientation. In the gas phase, circular dichroism was first observed in the photoionization of NO molecules that were aligned by multiphoton absorption into a well-defined excited state [15]. Circular dichroism has also been observed [16–20] in molecular-frame photoelectron angular distributions (MFPADs) of randomly oriented achiral molecules (hereafter called "circular dichroism in the angular distribution," CDAD). In this case, the three vectors can be unambiguously determined by detecting in coincidence photoions and photoelectrons that result from the one-photon dissociative ionization of the molecule. In experiments performed with homonuclear molecules [17,21,22], the CDAD has been found to be antisymmetric with respect to the polar electron emission angle θ_e [see Fig. 1(a)], which means that circular dichro-

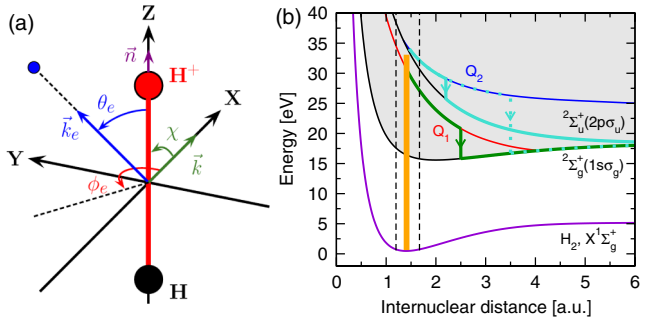

FIG. 1 (color online). (a) Molecular frame. The molecular axis is Z and the proton emission direction is $\mathbf{n}$. The light propagation direction is $\mathbf{k}$ (along the X axis). The electron is ionized in the direction $\Omega_e = (\theta_e, \phi_e)$ and has a momentum $\mathbf{k}_e$. All results shown in the following figures correspond to the YZ plane. (b) Potential energy curves of H_2 and H_2^+. $X^1\Sigma_g^+$ denotes the ground electronic state of H_2, and $^2\Sigma_g^+(1s\sigma_g)$ and $^2\Sigma_u^+(2p\sigma_u)$ the ground and the first excited electronic state of H_2^+. Q_1 and Q_2 denote the lowest $^1\Sigma_u^+$ and $^1\Pi_u$ doubly excited states above the $^2\Sigma_g^+(1s\sigma_g)$ and the $^2\Sigma_u^+(2p\sigma_u)$ threshold, respectively. Semiclassical paths (green and blue lines) describing autoionization of the Q_1 and Q_2 states after absorption of a 32.5 eV photon [thick vertical (orange) line] are shown.

ism vanishes when the MFPADs are integrated over that angle, i.e., when the electron angular distributions are not resolved in the polar emission direction.

In this Letter we show, by means of experiments and theoretical calculations, that circular dichroism in resonant dissociative photoionization of H_2 exhibits unusual properties that emerge from the control of electron emission in the molecular frame as a function of the kinetic energy (KE) of the emitted proton. In particular, for specific KEs and photon energies in the range 30–35 eV, the CDAD antisymmetry associated with homonuclear molecules disappears. Consequently, circular dichroism persists even when electron angular distributions are integrated over the polar emission direction. In addition, the present study probes the coherent interplay between the Σ and Π electronic states and the nuclear wave packets that are launched into the corresponding ionization and dissociation continua after absorption of a vacuum ultraviolet photon. The comparison with four-body (full dimensional) time-dependent calculations provides information about the relative emission times of autoionizing states of different symmetries in the femtosecond time scale.

The experiments were performed at the DESIRS beam line [23] at SOLEIL, operated in the eight-bunch mode (period 147 ns, time width 50 ps), using the vector correlation method [24]. The circular polarization rate s_3/s_0 of the light, where (s_0, s_1, s_2, s_3) are the Stokes parameters, was higher than 0.95. The light beam was crossed with a supersonic H_2 or D_2 gas jet (SAPHIRS) inducing photoionization in a narrow interaction volume. The ejected ions and electrons were guided to two time and position sensitive detectors by a dc electric field $\mathbf{E}$ coupled to a set of focusing lenses, whose magnitude, between 20 V/cm and 150 V/cm, ensured a 4π collection of both particles [25]. The $\mathbf{V}_H$ ionic fragment and $\mathbf{V}_e$ photoelectron emission velocity vectors were calculated from the impact times and positions for each (H^+, e) dissociative photoionization event. The electron-ion kinetic energy correlation derived from the ($\mathbf{V}_H$, $\mathbf{V}_e$) vector correlation provides the detailed energy sharing between the photoelectron energy (E_e) and the KE of the atomic fragments [8,24]. The coincident events assigned to the studied reaction are easily identified along a diagonal band which corresponds to the [H^+ + H(1s)] ground-state dissociation limit, at 18.1 eV above the $H_2(X^1\Sigma_g^+, v = 0)$ origin, which is the single one opened for the system in the explored photon excitation energies $h\nu \leq 35$ eV [8]. Selection of such events enables us to record the MFPAD as a function of the KE. The MFPAD, $I(\chi, \theta_e, \phi_e)$, is a function of the polar angle χ referring the orientation of the molecular axis $\mathbf{n}$ with respect to the light propagation axis $\mathbf{k}$, and the electron emission direction $\mathbf{k}_e(\theta_e, \phi_e)$ in the molecular frame defined by the molecular axis and the light propagation axis [19,22], as shown in Fig. 1(a). We use the data analysis reported in [19] to perform a fit of the $I(\chi, \theta_e, \phi_e)$ distribution and obtain the $I(\theta_e, \phi_e)$ MFPAD for any orientation (χ) of the fixed-in-space molecule. The CDAD is largest for scattering in a plane perpendicular to the light propagation axis ($\phi_e = 90°$ or 270°) that contains the molecular axis ($\chi = 90°$). In this plane, it is defined as the relative variation of the $I(\chi = 90°, \theta_e, \phi_e = 90°)$ MFPAD [or the $I(\chi = 90°, \theta_e, \phi_e = 270°)$] when the helicity of the light is changed from +1 (left-handed circular polarization) to −1 (right-handed circular polarization):

$$\mathrm{CDAD}(\theta_e) = [I_{+1}(\theta_e) - I_{-1}(\theta_e)]/[I_{+1}(\theta_e) + I_{-1}(\theta_e)]. \quad (1)$$

The CDAD takes values in the interval [− 1, 1].

The theoretical method used in our computations has been described elsewhere [26,27]. Briefly, we solve the time-dependent Schrödinger equation in which the laser-H_2 interaction is described in the dipole approximation. The laser field is represented by a pulse of 10 fs duration, temporal cosine-square envelope, and peak intensity 10^{12} W/cm^2. The pulse duration is large enough to represent the long duration of the radiation field used in the experiment [26,27]. All electronic and vibrational (dissociative) degrees of freedom are taken into account (7 dimensions). Thus, the calculations are performed in the real three-dimensional world (except for the nuclear rotation) and, therefore, include the effect of electron correlation and interferences between different ionization and dissociation pathways. In practice, the time-dependent Schrödinger equation is solved by expanding the time-dependent wave function in a large number of vibronic states that include the $^1\Sigma_u^+$ and $^1\Pi_u$ bound states of H_2, the $^2\Sigma_g^+(1s\sigma_g)$ and the $^2\Sigma_u^+(2p\sigma_u)$ ionization continua, and the doubly excited states embedded in them. Projection of this wave function onto vibronic states leads, without any ambiguity, to transition amplitudes that are easily combined [28] to yield the fully differential electron angular distributions. In contrast with simpler single-photon stationary methods (as those used, e.g., in [6]), solution of the time-dependent Schrödinger equation not only provides the desired transition amplitudes but also their time evolution. This is useful to unravel the dominant mechanisms responsible for the delayed ionization from the H_2 doubly excited states.

Figure 1(b) shows the potential energy curves [29,30] that are relevant to understand the physics of the different processes. Figure 2 shows the measured and calculated KE spectra for left-handed circularly polarized light of 19 and 32.5 eV. The theory provides the separate contribution of ionization into the $1s\sigma_g$ and $2p\sigma_u$ channels. Figure 2 also shows the measured and calculated MFPAD at selected proton energies. At 19 eV, the dominant process is direct ionization through the $1s\sigma_g$ state of the molecular ion [see Fig. 1(b)]. As Fig. 2(a) shows, this process is only relevant at very low KE, which is a consequence of the rapid decrease of the Franck-Condon overlap between the initial vibrational state of H_2 and the dissociative continuum of H_2^+. In this energy range, contributions from both the $^1\Sigma_u^+$

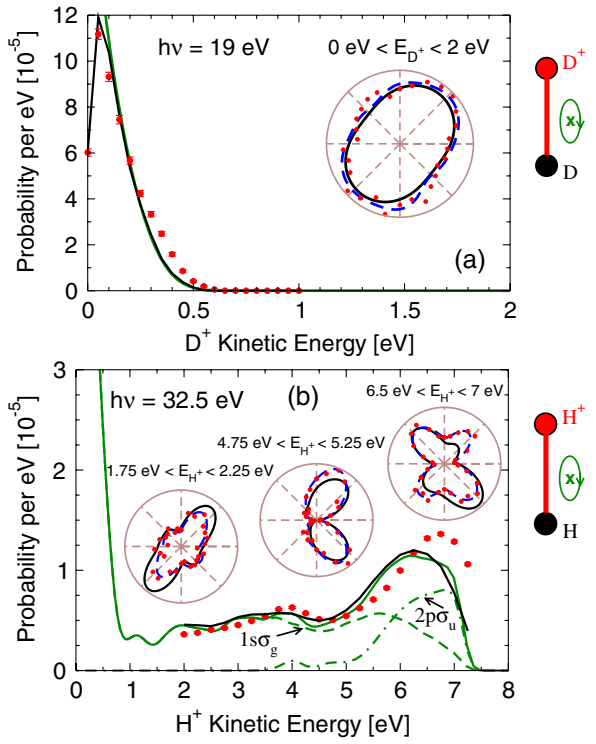

FIG. 2 (color online). Dissociative ionization probability as a function of deuteron (proton) kinetic energy for left-handed circularly polarized light. (a) D_2 with a photon energy of 19 eV. (b) H_2 with a photon energy of 32.5 eV. Insets: Polar plots of the MFPADs associated with the D^+ (H^+) kinetic energy intervals indicated in the figure. Red circles, experimental results normalized to theory; green solid line, theoretical results; black solid line, theoretical results convoluted with the instrumental resolution; blue dashed line in the insets, fit to the experimental results; green dashed line, dissociative ionization probability associated with the $1s\sigma_g$ channel; green dash-dotted line, the same associated with the $2p\sigma_u$ channel.

and $^1\Pi_u$ molecular symmetries are relevant, which leads to an electron angular distribution that is neither that of the $^1\Sigma_u^+$ electronic continuum nor that of the $^1\Pi_u$ one (when linearly polarized light is used, the latter two MFPADs are associated with molecules oriented parallel and perpendicular to the polarization direction, respectively). At 32.5 eV [see Fig. 2(b)], the KE spectrum is much more complex. In addition to the direct ionization process mentioned above, which appears at very low H^+ KEs, there is a significant ionization signal up to 7.5 eV. The latter signal is mostly due to autoionization (AI) of the $Q_1\,^1\Sigma_u^+$ [31] and $Q_2\,^1\Pi_u$ doubly excited states [32] [see Fig. 1(b)], as well as to direct ionization (DI) through the $2p\sigma_u$ channel. More specifically, the dominant processes that contribute to the KE spectrum at this photon energy are

$$H_2 \rightarrow H + H^+ + e^-(1s\sigma_g, {}^1\Sigma_u^+) \quad \text{DI}, \tag{2}$$

$$H_2 \rightarrow H + H^+ + e^-(1s\sigma_g, {}^1\Pi_u) \quad \text{DI}, \tag{3}$$

$$H_2 \rightarrow H_2^{**}(Q_1) \rightarrow H + H^+ + e^-(1s\sigma_g, {}^1\Sigma_u^+) \quad \text{AI}, \tag{4}$$

$$H_2 \rightarrow H + H^+ + e^-(2p\sigma_u, {}^1\Sigma_u^+) \quad \text{DI}, \tag{5}$$

$$H_2 \rightarrow H + H^+ + e^-(2p\sigma_u, {}^1\Pi_u) \quad \text{DI}, \tag{6}$$

$$H_2 \rightarrow H_2^{**}(Q_2) \rightarrow H + H^+ + e^-(1s\sigma_g, {}^1\Pi_u) \quad \text{AI}, \tag{7}$$

$$H_2 \rightarrow H_2^{**}(Q_2) \rightarrow H + H^+ + e^-(2p\sigma_u, {}^1\Pi_u) \quad \text{AI}, \tag{8}$$

where symbols within parenthesis indicate the ionization channel ($1s\sigma_g$ or $2p\sigma_u$) and the symmetry of the final electronic state ($^1\Sigma_u^+$ or $^1\Pi_u$). Processes (2) and (3) contribute to the low KE region (0–1 eV), process (4) contributes to all KE $>$ 1 eV, process (7) to the intermediate KE region (1–5 eV), and processes (5), (6), and (8) to the high KE region ($>$ 5 eV). Therefore, channels of $^1\Sigma_u^+$ and $^1\Pi_u$ symmetries overlap all throughout the KE spectrum, and consequently, the MFPADs differ from those obtained with linearly polarized light. Figure 2(b) shows the MFPADs at selected H^+ KEs. In spite of the rich structure of these angular distributions and of the fact that they rapidly vary with H^+ KE, the agreement between experiment and theory is good. As can be seen, for H^+ KE $>$ 4 eV, the MFPADs do not have inversion symmetry, in contrast with the MFPADs obtained at very low KE or for lower photon energies ($<$ 28 eV). As we will see, this naturally reflects in the CDAD.

Figure 3 shows the CDAD for the two photon energies and D^+ or H^+ kinetic energies considered in Fig. 2. As can be seen in Fig. 3(a), for a photon energy of 19 eV, circular dichroism is observed at all polar emission angles except for 0°, 90°, and 180° where it is exactly zero. The CDAD is perfectly antisymmetric with respect to 90°, in agreement with previous results for N_2 [17] and O_2 [21]. In contrast, Fig. 3(b) shows that, for a photon energy of 32.5 eV, the CDAD may not be antisymmetric with respect to 90°. This is particularly true for KE energies between 4 and 7 eV where autoionization leaves H_2^+ in both the $1s\sigma_g$ and $2p\sigma_u$ states with a significant probability [see

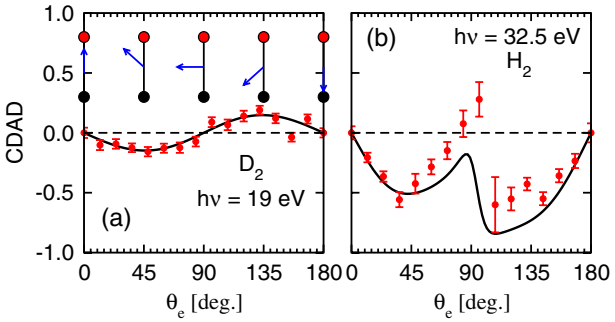

FIG. 3 (color online). CDAD. Red circles: experimental results. Black curves: theoretical results convoluted with the instrumental resolution. (a) Results for D_2, a photon energy of 19 eV, and deuteron energies 0–2 eV. (b) Results for H_2, a photon energy of 32.5 eV, and proton energies 4.75–5.25 eV. The red balls in the insets of (a) denote D^+, and the black ones, D; the blue arrow indicates the electron emission direction.

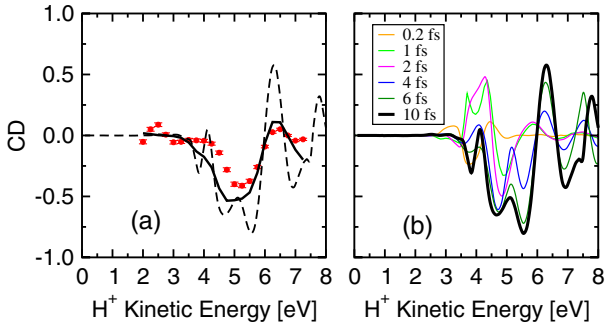

FIG. 4 (color online). Circular dichroism (CD) associated with MFPADs integrated over θ_e for H_2 and a photon energy of 32.5 eV. (a) Red dots, experimental results; black dashed line, theoretical results; black solid line, theoretical results convoluted with the experimental energy and angular resolution. (b) Variation of the calculated CD with the integration time used to solve the time-dependent Schrödinger equation.

Fig. 2(b)]. As a consequence, circular dichroism associated with θ_e-integrated MFPADs (CD for short) is significantly different from zero between 4 and 7 eV [see Fig. 4(a)]. In this region, the probability of ionization into the $1s\sigma_g$ and $2p\sigma_u$ channels is comparable, which leads to a coherent superposition of the $1s\sigma_g$ and $2p\sigma_u$ states of H_2^+ [6].

Figure 4(b) shows the computed time evolution of the CD. It can be seen that, at very short integration times ($t <$ 0.2 fs), the CD is practically zero for all H^+ KEs. At such short times, autoionization from the Q_1 and Q_2 doubly excited states through processes (4), (7), and (8) has not yet occurred and the CDAD is antisymmetric with respect to 90°. As t approaches 1 fs, the CD rapidly becomes different from zero and remains more or less unchanged between 1 and 2 fs. Later on, the CD changes again and converges to its final value at around 5–6 fs. The two different time scales correspond to two different mechanisms. The fast one involves autoionization from the $Q_1\,^1\Sigma_u^+$ and $Q_2\,^1\Pi_u$ states into, respectively, the $1s\sigma_g$ and $2p\sigma_u$ channels [processes (4) and (8)]. The interference between the latter channels leads already to a nonzero CD. The slow mechanism corresponds to autoionization from the $Q_2\,^1\Pi_u$ state into the $1s\sigma_g$ channel [process (7)], which modifies the pattern of the interference and hence the CD. These time scales are compatible with the known autoionization lifetimes of these three channels in the Franck-Condon region [29,30].

In conclusion, the observation in homonuclear molecules of circular dichroism in the photoelectron angular distributions integrated over the polar emission angle is the signature of delayed autoionization into channels of different inversion symmetry. Thus, measuring circular dichroism is a sensitive probe for the identification of molecular autoionizing states in such molecules. In particular, fs circularly polarized pulses might be the ideal tool to characterize the autoionization dynamics.

We thank MareNostrum BSC and CCC-UAM for computer time. Work was supported by the MICINN Projects No. FIS2007-60064, No. ACI2008-0777, and No. CSD2007-00010, the European COST Action CM0702, the Universidad de Antioquia, the Colciencias Agency, and the Alban Program. We gratefully acknowledge the cooperation of L. Nahon and his group at SOLEIL, and S. Damoy at the LCAM. D. D. is very grateful to R. R. Lucchese for communication of unpublished calculations for direct ionization and to M. Lebech for his contribution in early experiments at SACO.

[1] J. Ullrich, R. Moshammer, A. Dorn, R. Dörner, L. P. H. Schmidt, and H. Schmidt-Böcking, Rep. Prog. Phys. **66**, 1463 (2003).
[2] D. Akoury *et al.*, Science **318**, 949 (2007).
[3] B. Zimmermann *et al.*, Nature Phys. **4**, 649 (2008).
[4] D. Rolles *et al.*, Nature (London) **437**, 711 (2005).
[5] J. Fernández, O. A. Fojón, A. Palacios, and F. Martín, Phys. Rev. Lett. **98**, 043005 (2007).
[6] F. Martín *et al.*, Science **315**, 629 (2007).
[7] M. S. Schöffler *et al.*, Science **320**, 920 (2008).
[8] A. Lafosse *et al.*, J. Phys. B **36**, 4683 (2003).
[9] P. Atkins and J. de Paula, *Elements of Physical Chemistry* (Oxford University Press, New York, 2005), 4th ed..
[10] N. A. Cherepkov, Chem. Phys. Lett. **87**, 344 (1982).
[11] R. L. Dubs, S. N. Dixit, and V. McKoy, Phys. Rev. Lett. **54**, 1249 (1985).
[12] N. A. Cherepkov and V. V. Kuznetsov, Z. Phys. D **7**, 271 (1987).
[13] C. Westphal, J. Bansmann, M. Getzlaff, and G. Schönhense, Phys. Rev. Lett. **63**, 151 (1989).
[14] C. Westphal, A. P. Kaduwela, C. S. Fadley, and M. A. Van Hove, Phys. Rev. B **50**, 6203 (1994).
[15] K. L. Reid, D. J. Leahy, and R. N. Zare, Phys. Rev. Lett. **68**, 3527 (1992).
[16] S. Motoki *et al.*, J. Phys. B **35**, 3801 (2002).
[17] T. Jahnke *et al.*, Phys. Rev. Lett. **88**, 073002 (2002).
[18] O. Geßner *et al.*, Phys. Rev. Lett. **88**, 193002 (2002).
[19] M. Lebech *et al.*, J. Chem. Phys. **118**, 9653 (2003).
[20] M. Lebech, J. C. Houver, D. Dowek, and R. R. Lucchese, Phys. Rev. Lett. **96**, 073001 (2006).
[21] D. Dowek, M. Lebech, J. C. Houver, and R. R. Lucchese, J. Electron Spectrosc. Relat. Phenom. **141**, 211 (2004).
[22] D. Dowek, M. Lebech, J. C. Houver, and R. R. Lucchese, Mol. Phys. **105**, 1757 (2007).
[23] L. Nahon *et al.*, Rev. Sci. Instrum. **72**, 1320 (2001).
[24] A. Lafosse *et al.*, Phys. Rev. Lett. **84**, 5987 (2000).
[25] M. Lebech, J. C. Houver, and D. Dowek, Rev. Sci. Instrum. **73**, 1866 (2002).
[26] A. Palacios, H. Bachau, and F. Martín, Phys. Rev. Lett. **96**, 143001 (2006).
[27] J. L. Sanz-Vicario, H. Bachau, and F. Martín, Phys. Rev. A **73**, 033410 (2006).
[28] J. F. Pérez-Torres, F. Morales, J. L. Sanz-Vicario, and F. Martín, Phys. Rev. A **80**, 011402(R) (2009).
[29] I. Sánchez and F. Martín, J. Chem. Phys. **106**, 7720 (1997).
[30] I. Sánchez and F. Martín, J. Chem. Phys. **110**, 6702 (1999).
[31] I. Sánchez and F. Martín, Phys. Rev. Lett. **79**, 1654 (1997).
[32] I. Sánchez and F. Martín, Phys. Rev. Lett. **82**, 3775 (1999).